Int. J. Fracture manuscript No.
(will be inserted by the editor)

A fast algorithm to simulate the failure of a periodic elastic fibre composite

Sivasambu Mahesh, Ankit Gupta, Uttam S. Kachhwah, Najam Sheikh

Received: date / Accepted: date

Abstract Monte-Carlo simulations of the fracture of elastic unidirectional model fibre composites are an important tool to understand composite reliability. On account of being computationally intensive, fracture simulations reported in the literature have been limited to composite patches comprised of a few thousand fibres. While these limited patch sizes suffice to capture the dominant failure event when the fibre strength variability is low (synthetic fibres), they suffer from edge effects when the fibre strength variability is high (natural fibres). On the basis of recent algorithmic developments based on Fourier acceleration, a novel bisection based Monte Carlo failure simulation algorithm is presently proposed. This algorithm is used to obtain empirical strength distributions for model composites comprised of up to $2^{20} \approx 10^6$ fibres, and spanning a wide range of fibre strength variability. These simulations yield empirical weakest-link strength distributions well into the lower tail. A stochastic model is proposed for the weakest-link event. The strength distribution predicted by this model fits the empirical distributions for any fibre strength variability.

Keywords Composites; Fracture; Algorithm; Discrete Fourier Transform; Numerical methods

1 Introduction

Randomness in fibre strengths causes variability in the strengths of nominally identical unidirectional fibre composite specimen (Hull and Clyne 1996). The relationship between the distribution of the fibre strengths, and that of composite strength depends on the nature of load redistribution from intact to broken fibres, termed the load-sharing rule. Much work in the literature has been directed toward understanding this relationship, for various load-sharing rules (Smith 1980; Beyerlein et al 1996; Zhou and Curtin 1995; Curtin 1998; Landis et al 2000; Mahesh et al 1999, 2002; Habeeb and Mahesh 2015). A commonality amongst these works is the use of Monte Carlo simulations of composite fracture, for deriving insight into the fracture of these materials.

Monte Carlo fracture simulations have established that the distribution of strength per fibre, σ, of N-fibre composites, $G_N(\sigma)$, obeys weakest-link scaling (Smith 1980; Beyerlein et al 1996; Curtin 1998; Landis et al 2000; Mahesh et al 1999, 2002; Gupta et al 2017b), i.e., for large enough N, there exists a function $W(\sigma)$, independent of N, such that

$$G_N(\sigma) = 1 - (1 - W(\sigma))^N. \tag{1}$$

When the variability of fibre strength is small, as in the case of commercial synthetic fibres, Eq. (1) is already satisfied for relatively small composite sizes, N. However, the fibre strength variability in natural fibre composites and in hybrid composites, wherein two or more types of fibre reinforcements are used, is typically large (Jawaid and Khalil 2011; Fidelis et al 2013). In this case, Eq. (1) is valid only for very large N. Thus, for such composites, Monte Carlo simulations of large composite patch sizes (N) are necessary to obtain $W(\sigma)$.

The number of fibres in a standard unidirectional ASTM D3039 test coupon (ASTM 2017) is of the order of $N \sim 10^6$. Linear load sharing models (Hedgepeth 1961; Hedgepeth and Van Dyke 1967; Zhou and Curtin 1995) assume a linear elastic matrix, and a perfectly

Sivasambu Mahesh (✉) · Ankit Gupta · Uttam S. Kachhwah · Najam Sheikh
Department of Aerospace Engineering, Indian Institute of Technology Madras, Chennai 600 036, India.
E-mail: smahesh@iitm.ac.in

bonded interface. By virtue of the linearity of the governing equations, superposition of break influences is permissible (Beyerlein et al 1996). This enables the simulation of the fracture of composite patches comprised of several hundreds, to a few thousands of fibres (Curtin 1998; Landis et al 2000; Mahesh et al 2002). Linear models neglect the material non-linearities present in physical composites.

To overcome this deficiency, non-linear load sharing models that account for matrix plasticity, matrix fracture, interfacial debonding and sliding are available in the literature, e.g., Landis and McMeeking (1999); Okabe et al (2001); Okabe and Takeda (2002), and Mishra and Mahesh (2017). The non-linear character of these models disallows the superposition of solutions due to individual failure events (Mahesh and Mishra 2018). As a consequence, fracture simulations must be restricted to small composite patches (Zhang and Wang 2009; Mahesh and Mishra 2018), comprised of several tens, to a few hundred fibres. Unsurprisingly, the problem of achieving realistic composite sizes in fracture simulations is much more challenging for the case of non-linear models, than for linear models. The latter is therefore the focus of the present work.

Enhancements in computer technology, particularly, processor speeds, and the multi-core architecture of the present processors, help in reaching larger patch sizes, to some extent. Presently, one Monte Carlo simulation of a composite patch comprised of about $N = 10^4$ fibres can be performed by a generic four-core processor, in a day. But this is still two orders of magnitude smaller than the typical number of fibres in a standard test coupon. Simulations of larger patches is difficult because, the computational complexity of the Monte-Carlo simulation even in a linear model composite is $O(N^3)$, as shown later.

The foregoing reasons motivate improvements in the algorithms for performing Monte Carlo simulations. In a model linear composite, Gupta et al (2017b) observed that the most computationally intensive step in the Monte Carlo simulations is the computation of the interactions amongst breaks. They sought to reduce the computational cost of this step by accounting exactly for the interactions amongst nearby breaks, but only approximately for that between distant breaks. They implemented this notion using a tree code algorithm. Using this devise, Gupta et al (2017b) could simulate the failure of composite patches comprised of up to $N = 2^{16} \approx 65000$ fibres.

A limitation of the tree code algorithm of Gupta et al (2017b) is that an approximation error is introduced when accounting for the interactions between distant breaks. This error is difficult to mathematically bound; Gupta et al (2017b) demonstrated the smallness of the approximation error by considering several critical test cases. Another limitation is that simulation patches with $N > 2^{16}$ were inaccessible to the quadtree algorithm. For this reason, Gupta et al (2017b), could not establish the validity of Eq. (1) for a case of very large fibre strength variability. A numerically exact algorithm, capable of simulating even larger composite patches would be desirable. The building blocks of such an algorithm, based on the notion of Fourier acceleration (Batrouni et al 1986), have been developed by Gupta et al (2017a) and Gupta et al (2018).

The present work summarises this development and proposes a novel Monte Carlo simulation algorithm that exploits their computational features. The developed algorithm has a computational complexity of $O(N \log N)$. That is, keeping all other model parameters fixed, the computational effort associated with obtaining the composite strength for a given set of fibre strength scales with N as $N \log N$ (Cormen et al 2001). It is used to simulate the failure of model composite patches comprised of up to $N = 2^{20} \approx 10^6$ fibres. From these simulations, the empirical $W(\sigma)$ can be readily derived from Eq. (1), for all the fibre strength variabilities studied. A two-parameter stochastic model of the weakest-link event is also proposed. The model $W(\sigma)$ is shown to fit the empirically obtained $W(\sigma)$ very well, for all fibre strength variabilities. The proposed model can be used to calculate the strength distribution $G_N(\sigma)$ of the composite to very high reliability levels.

2 Model and algorithm

2.1 Fibres

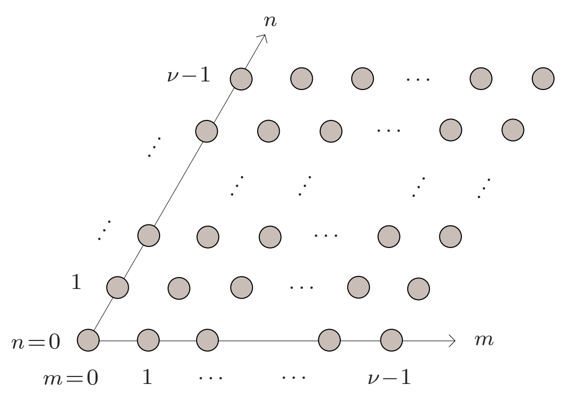

Fig. 1: A rhombus-shaped periodic patch of $\nu \times \nu$ fibers arranged in a hexagonal lattice showing the m–n coordinate system.

The model composite is comprised of $N = \nu \times \nu$ infinitely-long aligned fibres, arranged in a hexagonal lattice, as shown in Fig. 1. Fibres are located by their (m, n) coordinates, as shown. Periodic boundary conditions are imposed in the transverse direction at the edges of the patch, as detailed in Gupta et al (2017a, 2018).

Following Gücer and Gurland (1962), Smith (1980), and Smith et al (1983), the composite is divided in the fibre-direction into a chain-of-bundles. The length of each bundle is assumed to be the ineffective length, δ, given by Hedgepeth (1961).

The random strength, Σ, of a fibre element depends on its length, l, and follows the Weibull (1951) distribution (Hull and Clyne 1996):

$$\Pr\{\Sigma \leq \sigma\} = 1 - \exp\left(-(l/l_0)(\sigma/\sigma_0)^\rho\right), \tag{2}$$

where l_0 is a reference gage length, and ρ denotes the Weibull exponent. The exponent ρ determines the variability of fibre strength: with increasing ρ, the fibre strength variability decreases. The fibre gage length of present interest is that contained in a bundle. Thus, $l = \delta$. Defining normalised versions of Σ, and σ as:

$$X = \Sigma\ (\delta/l_0)^{1/\rho}/\sigma_0, \text{ and } x = \sigma\ (\delta/l_0)^{1/\rho}/\sigma_0, \tag{3}$$

allows rewriting Eq. (2) as:

$$F(x) := \Pr\{X \leq x\} = 1 - \exp\left(-x^\rho\right). \tag{4}$$

Here, the notation ':=' indicates the definition of $F(x)$.

By suitably non-dimensionalising the fiber-wise positional coordinate, and axial displacements, Hedgepeth (1961) showed that the governing equations may be freed of all material parameters. This approach has been adopted in the literature since (Mahesh et al 1999; Landis et al 2000). Let $u_{mn}(\zeta)$ denote the normalised displacement of fibre (m, n) in the fiber direction, at normalised fibre-wise positional coordinate, ζ. The governing equilibrium equations along the fibre direction, following Hedgepeth (1961) are

$$\frac{d^2 u_{mn}}{d\zeta^2}(\zeta) + \sum_p \sum_q A_{mnpq} u_{pq}(\zeta) = 0. \tag{5}$$

All the indices in Eq. (5) range over $\{0, 1, \ldots, \nu\}$, and

$$A_{mnpq} = \begin{cases} -6, & \text{if } p = m, \text{ and } q = n, \\ 1, & \text{if } p = [m \pm 1], \text{ and } q = n, \\ 1, & \text{if } p = m, \text{ and } q = [n \pm 1], \\ 1, & \text{if } p = [m \pm 1], \text{ and } q = [n \mp 1], \\ 0, & \text{otherwise.} \end{cases} \tag{6}$$

In Eq. (6), the notation $[m]$ is defined as $[m] := m - \nu \lfloor m/\nu \rfloor$.

2.2 Interacting fibre breaks

Consider the bundle containing the plane $\zeta = 0$. Let N_b of the N fibres be broken. Indexing the fibre at (m, n) as $i = m\nu + n + 1$, let the indices of the broken fibres be $\{i_1, i_2, \ldots, i_{N_b}\}$. Let these fibre breaks be confined to the plane $\zeta = 0$. This is a conservative assumption, as the stress concentration due to breaks in a transverse plane always exceed that due to axially staggered breaks (Smith 1980; Mahesh et al 1999).

The overloads in the $N - N_b$ intact fibres due to the breaks is determined in three steps (Landis et al 2000; Mahesh et al 1999). First, the overloads due to a single break are determined, using the fast $O(N \log N)$ algorithm due to Gupta et al (2017a). Second, for the case that multiple breaks are present, their weights, w_{i_k}, $k \in \{1, 2, \ldots, N_b\}$, which physically represent their opening displacements are determined by solving a system of N_b linear equations at a cost of $O(N_b^3)$. This cost can be reduced to $O(N_b^2)$ if the inverse of the coefficient matrix corresponding to $N_b - 1$ breaks is stored (Landis et al 2000). An alternate algorithm, based on the iterative conjugate gradient method, and Fourier acceleration, was proposed to solve this problem. The method has a computational complexity of $O(N \log N)$ (Gupta et al 2018). It was found that the latter method was faster than the former for N_b in excess of a few hundred fibre breaks. Third, the overloads due to the individual breaks are weighted and superposed to obtain the overloads in all the intact fibres. The classical computational cost of this operation, $O(NN_b)$, is reduced to $O(N \log N)$ using Fourier acceleration (Gupta et al 2018).

Thus, the algorithm proposed by Gupta et al (2018) replaces the $O(N_b^2 + NN_b)$ complexity of determining the overloads on the intact fibres due to a system of breaks, by one with $O(N \log N)$ complexity.

2.3 Monte Carlo simulation

The classical algorithm of the Monte Carlo simulations have been described by a number of authors, e.g., Landis et al (2000). In this algorithm, fibre strengths are randomly drawn from Eq. (4). The far-field load is increased just enough to break the weakest fibre. The stress overloads on the remaining $N - N_b = N - 1$ fibres are computed. The far-field load is updated (increased or decreased) so that exactly one more fibre will fail, but this time, under the influence of the stress concentrations produced by the pre-existing broken fibre. The weights of the $N_b = 2$ interacting breaks are determined, and the stress overloads on the $N - N_b = N - 2$

intact fibres is updated to reflect their stress concentration. This process is repeated until all the fibres are broken, i.e., $N_b = N$.

Since the computational effort of evaluating the stress overloads after the breakage of each fibre, using the classical Monte Carlo algorithm, is $O(N_b^2 + NN_b)$, the computational effort associated with a Monte Carlo simulation would be $O(N^3)$. If, instead, the stress overloads were updated following the Fourier accelerated algorithms (Sec. 2.2), the computational effort of the resulting Monte Carlo simulation algorithm would be $O(N)O(N \log N) = O(N^2 \log N)$. This would improve upon the classical $O(N^3)$ algorithm, but it is possible to do even better.

The present algorithm tests whether or not the model composite will break under a constant imposed normalised far-field load per fibre, x, given by Eq. (3). In the first step, all the fibres whose normalised strengths X are smaller than x are broken. The set of all broken fibres at this step constitutes the first 'burst', in the terminology of Alava et al (2006). The overloads on the intact fibres is determined using the $O(N \log N)$ computation of Sec. 2.2. If the overload causes of any of the intact fibres to fail as part of the second burst, those breaks are added. This process is repeated through the third burst, fourth burst, and so on, until no more fibres fail. If the process terminates with intact fibres remaining in the patch, the constant force applied per fibre, x, is smaller than the strength of the composite. If, on the other hand, the application of x produces breaks in all the fibres, the composite strength is smaller than x. The computational effort associated this test is still $O(N \log N)$, with a pre-factor proportional to the number of bursts.

The actual strength of the composite is determined using successive bisection. The strength per fibre of the composite is initially bracketed to lie in the interval $[\underline{x}, \overline{x}]$. $\underline{x}$ and $\overline{x}$ can be taken as the normalised strengths of the weakest and strongest fibres in the simulation patch, respectively. Alternately, a tighter bracket is obtained if $\underline{x}$ and $\overline{x}$ were taken to correspond to the strength per fibre of a 1D local load sharing tape, and that of an equal load sharing bundle. The fibres in these two 'bounding composites' are assigned the same strengths as the fibres of the present simulation. An efficient algorithm for determining $\underline{x}$ was given by Mahesh and Phoenix (2004). As for the strength $\overline{x}$ of the equal load sharing bundle, even a naive algorithm is adequate.

After the bracket is constructed, the composite is tested for failure at its mid-point, which corresponds to an applied normalised far-field load per fibre of $(\underline{x} + \overline{x})/2$. If the composite fails, $\overline{x}$ is updated to $(\underline{x} + \overline{x})/2$; otherwise, $\underline{x}$ is updated to $(\underline{x} + \overline{x})/2$. This process is repeated until the size of the bracket becomes smaller than a prescribed tolerance, ε:

$$\overline{x} - \underline{x} < \varepsilon. \tag{7}$$

For sufficiently small ε, it has been verified that the set of broken fibres formed before the final burst, following the present algorithm, coincides with the set of fibres broken just before the peak load is achieved, as predicted by the classical simulation algorithm.

The computational effort of this algorithm is the number of successive bisections times the computational effort of one test. The number of successive bisection steps depends on the ratio of the width of the initial bracket and ε, and not on the number of fibres, N. That is, if the initial bracket is wider, it can, at worst, slow down the composite strength computation by a constant factor independent of N. Therefore, the computational complexity of the Monte Carlo algorithm is also only $O(N \log N)$.

The presently proposed approach to determine the strength of a computer composite specimen is only efficient if paired with the $O(N \log N)$ Fourier accelerated algorithm for the computation of overloads (Gupta et al 2018). The classical simulation algorithm (Mahesh et al 1999; Landis et al 2000) is more efficient with the classical $O(N_b^2)$ algorithm for overloads computation.

3 Results and discussion

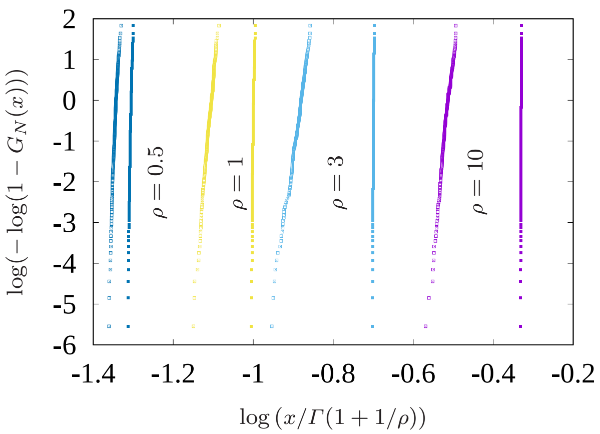

Fig. 2: Empirical strength distributions of Hedgepeth and equal load sharing composite patches comprised of $N = 2^{20}$ fibres obtained from $n_{\text{sim}} = 256$ simulations. Distributions corresponding to $\rho = 0.5$, 1, 3, and 10 are shown.

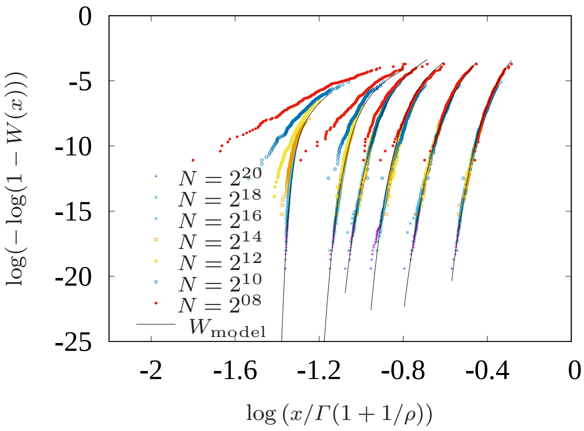

Fig. 3: Weakest-link strength distributions, calculated according to Eq. (1), for all the (ρ, N) pairs simulated. From left to right, the distributions correspond to $\rho = 0.5$, 1, 2, 3, 5, and 10. It is seen that for large enough N, the weakest-link strength distribution becomes independent of N, indeed. $\Gamma(1+1/\rho)$, the mean strength of the normalised distribution, Eq. (4), is used to normalise the abscissae.

The above algorithm is implemented in `GNU octave` (Eaton et al 2015), and run on a computer assembled by pairing a six-core Intel Core$^{\text{TM}}$ i7 8700 processor with a compatible motherboard, and 8 gigabytes of RAM. Five Monte-Carlo simulations are run simultaneously using `GNU parallel` (Tange 2011). For each $\rho \in \{0.5, 1, 2, 3, 5, 10\}$, $n_{\text{sim}} = 256$ simulations are run. Simulation time increases with decreasing ρ. This is because more numerous, albeit smaller, bursts of breaks occur at smaller ρ. Even so, the typical $\rho = 0.5$ simulation of the largest patch comprised of $N = 2^{20}$ fibres takes only about two hours of wall-clock time to complete. The strength of each simulated composite is determined to an accuracy of $\varepsilon = 10^{-3}$ in Eq. (7).

Fig. 2 shows the empirical strength distributions, $G_N(x)$, obtained from $n_{\text{sim}} = 256$ Monte Carlo simulations for $N = 2^{20}$ fibre composites with $\rho = 0.5$, 1, 3, and 10. Empirical strength distributions for two types of load sharing as shown: the Hedgepeth load sharing of Sec. 2.1 and equal load sharing. For all ρ, the latter results in stronger composites than the former. This is to be expected because in equal load sharing, the fibres near a break are not overloaded as severely as in Hedgepeth load sharing.

It is also seen that as ρ decreases, the empirical strength distribution obtained from equal load sharing approaches that obtained assuming Hedgepeth load sharing. Again, this is to be expected, as in the limit $\rho \to 0$, composite strength will be determined by the strength of the strongest fibres, regardless of the load sharing scheme.

The empirical weakest-link distributions,

$$W_N(x) = 1 - (1 - G_N(x))^{1/N}, \tag{8}$$

are deduced from the empirical strength distributions, $G_N(x)$ for $N = 2^8, 2^{10}, \ldots, 2^{20}$. These are plotted in Fig. 3. For $\rho = 10$, 5, 3, and 2, $W_N(x)$ are seen to be independent of N, for $N \geq 2^8$. That is, $W_N(x)$ is independent of N, in accord with Eq. (1), already at $N = 2^8$. However, for $\rho = 1$, $W_N(x)$ becomes independent of N, only for $N \geq 2^{12}$. For $\rho = 0.5$, the critical threshold for N-independence increases to $N \geq 2^{16}$. This result was not accessible to Gupta et al (2017b) as their largest simulation patch consisted of $N = 2^{16}$ fibres.

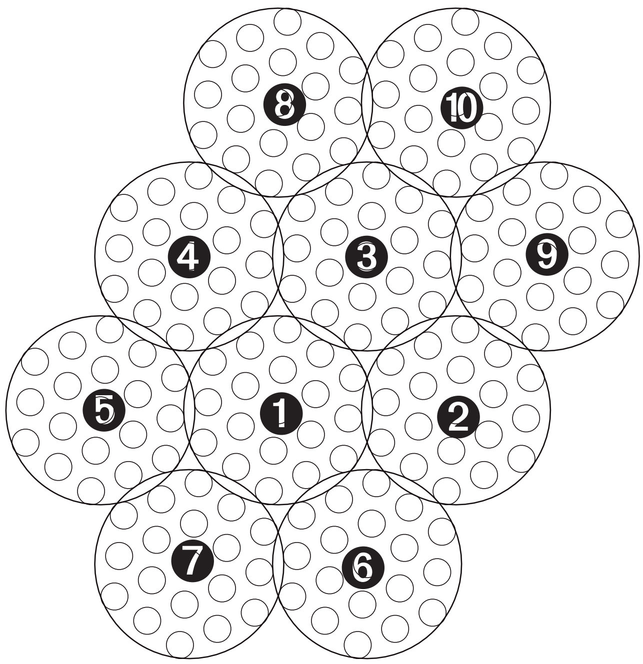

Fig. 4: Schematic representation of the failure event hypothesised to be the weakest-link event. The composite cross-section is viewed as a patch-work of bundles. In this figure, each bundle is comprised of 19 fibres, obeying equal-load sharing. The failure of a bundle, labelled ❶, causes an overload in its six neighbours. Under this overload, one of them, say ❷ fails. The overloads due to a pair of failed bundles leads to the failure of, say ❸, and so on.

A stochastic model, developed by Habeeb and Mahesh (2015), and Gupta et al (2017b), is now modified to explain the empirical weakest-link distributions, $W(x)$. In this model, the composite cross-section is viewed as a non-overlapping patch-work of equal load sharing bundles, each comprised of M fibres. This is shown in Fig. 4. It is proposed that $W(x)$ is the probability of sequential failure of neighbouring fibre bundles, wherein the next bundle to fail is one of those most severely overloaded by the present collection of failed bundles. This is illustrated in Fig. 4 up to the failure of the tenth bundle.

To obtain an expression for $W(x)$, expressions are required for the stress concentration due to broken bundles on their neighbours, and the number of most overloaded neighbours of a cluster of bundles. To this end, bundles are regarded as being arranged in 'rings', following Smith et al (1983), around a central bundle. The first ring is taken to contain only the central bundle. The second ring contains 6 bundles, the third ring, 12 bundles, and so on. The total number of bundles in r rings is given by $k = 1+6+\ldots+6(r-1) = 3r(r-1)+1$. Inverting this gives the number of rings corresponding to k bundles as

$$r = \left(1 + \sqrt{1 + 4(k-1)/3}\right) \Big/ 2. \tag{9}$$

Eq. (9) is strictly valid only when the rings are filled, e.g., for $k \in \{1, 7, 19, \ldots\}$. However, it is taken to be approximately valid for all k. The number of most overloaded neighbouring bundles around a cluster of r rings, comprised of k bundles, is given by $N_k = 6r$. These bundles are located at the size mid-sides of the outer most hexagonal ring. Again, although this formula is strictly true only for $k \in \{1, 7, 19, \ldots\}$, its approximate validity is assumed for all k.

The stress concentration due a tight cluster of k broken fibres on its most overloaded neighbours is given by (Mahesh et al 1999) $\sqrt{r/\pi + 1}$, where r is given by Eq. (9), in terms of k. The stress concentration, K_k, due to a cluster of k broken bundles on its most overloaded neighbouring bundle is also taken to follow the same scheme. In this view, the spatial variation of stess concentrations within a bundle is neglected. To account for this, a ρ-dependent scaling parameter, C is introduced:

$$K_k = C\sqrt{\frac{r}{\pi} + 1}. \tag{10}$$

Let $E_M(x)$ denote the strength distribution of an equal load sharing bundle of M fibres under imposed far-field normalised load x per fibre. A recursive expression for $E_M(x)$ has been given by McCartney and Smith (1983). This expression can be used up to about $M = 1000$. For $M > 1000$, round-off errors affect the recursion calculation. In this regime, the asymptotic expression for $E_M(x)$ as $M \to \infty$, due to Daniels (1945), provides a good approximation for $E_M(x)$.

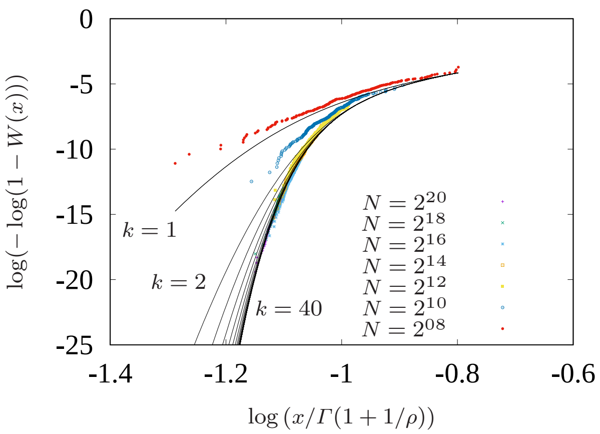

Fig. 5: Comparison of the empirical weakest link strength distribution with the model predicted $W_k(x)$ for $k = 1, 2, \ldots, 40$. $W_k(x)$ converges at about $k = 10$.

Table 1: Parameters of the probabilistic model used to obtain $W_{\text{model}}(x)$, in Fig. 3.

ρ	C_ρ	M_ρ
0.5	0.85	12000
1	0.87	200
2	0.89	20
3	0.94	20
5	0.95	3
10	1.075	1

In terms of $E_M(x)$, the probability of forming a tight cluster of $(k+1)$-bundles can be written as (Habeeb and Mahesh 2015; Gupta et al 2017b):

$$\hat{W}_{k+1}(x) = E_M(x)\left(1 - (1 - E_M(K_1 x))^{N_1}\right) \times \ldots \\ \ldots \times \left(1 - (1 - E_M(K_k x))^{N_k}\right). \tag{11}$$

Here, $E_M(x)$ is the probability of failure of the first bundle, and $1 - (1 - E_M(K_k x))^{N_k}$ is the probability of failure of at least one of the N_k most overloaded neighbours of a tight cluster of k bundles, each experiencing a stress concentration of K_k due to the tight cluster. Catastrophic failure corresponds to the continuous extension of the tight cluster, so that the probability of failure of the composite patch beginning with the failure of a fixed initial bundle is given by

$$\hat{W}(x) = \lim_{k\to\infty} \hat{W}_k(x). \tag{12}$$

The first bundle to fail can be any one of the N/M such bundles in the composite patch. Accordingly, the probability of failure of the composite patch is:

$$G_N(x) = 1 - (1 - \hat{W}(x))^{N/M}. \tag{13}$$

Comparing Eqs. (1), and (13) reveals that

$$\hat{W}(x) = 1 - (1 - W(x))^M. \tag{14}$$

Analogously,

$$\hat{W}_k(x) = 1 - (1 - W_k(x))^M \tag{15}$$

is also defined.

Fig. 5 compares $W_k(x)$, $k \in \{1, 2, \ldots, 40\}$ with the empirical weakest-link strength distribution obtained from Monte Carlo simulations, for the $\rho = 1$ composite patch. It is seen that $W_{40}(x)$ captures the empirical distributions very well. Two parameters are fit to obtain this coincidence: the bundle size, $M_1 = 200$ fibres, and $C_1 = 0.87$, in Eq. (10). Increasing M_ρ increases the curvature of W_k, while increasing C_ρ shifts W_k upward. It is seen from Fig. 5 that over the stress-range of interest, $W_k(x)$ has already converged to $W(x)$ for $k < 40$.

$W(x)$ can be determined for all the ρ by fitting the two ρ-dependent parameters M_ρ, and C_ρ, as listed in Table 1. The predicted $W(x)$ distributions are plotted in Fig. 3. These are seen to agree well with the empirical distributions obtained from the Monte Carlo simulations. The present model fits the empirical distributions well even in the upper tail, which is not true of the fits obtained by Gupta et al (2017b, Fig. 9). This suggests that the present approach to accounting for the stress concentrations due to failed equal load sharing bundles on their neighbours and the number of severely overloaded neighbours is more realistic. The present values of C_ρ and M_ρ are also considerably greater than those reported by Gupta et al (2017b).

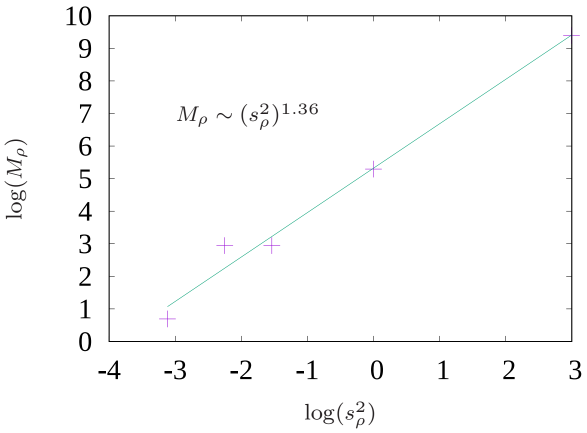

Fig. 6: The size of the equal load sharing bundle, M_ρ, scales as a power of the fibre strength variance, s_ρ^2.

It has been attempted to understand the physical basis for the variation of M_ρ with ρ. The hypothesis that the variance in the strength of M_ρ bundles would be approximately constant with ρ was found to be false. However, the variance associated with the fibre strength distribution, $F(x)$ (Eq. (4)),

$$s_\rho^2 = \Gamma(1 + 2/\rho) - \Gamma^2(1 + 1/\rho), \tag{16}$$

where $\Gamma(\cdot)$ denotes the gamma function is found to be related to M_ρ. Fig. 6 compares the bundle size, M_ρ with the fibre strength variance, s_ρ^2. It is seen that the bundle size, M_ρ, scales as a power of the fibre strength variance: $M_\rho \sim (s_\rho^2)^{1.36}$. A physical basis for this scaling is, however, not presently understood.

4 Conclusion

A computationally efficient bisection based $O(N \log N)$ Monte Carlo simulation algorithm for the failure of a composite patch obeying a realistic linear load sharing rule has been proposed. The algorithm is used to simulate the failure of composite patches comprised of up to $N = 2^{20}$ fibres for a range of fibre Weibull exponents ρ. The simulations reveal that the composite strength distribution obeys weakest-link scaling regardless of fibre strength variability. A model that explains the weakest-link strength distribution has also been proposed. This model regards the composite patch as a patch-work of equal load sharing bundles, each comprised of M_ρ fibres, which fail in response to overloads due to the failure of their neighbouring bundles. This model improves upon the model of Gupta et al (2017b), in that it captures the entire empirical distribution of the weakest-link strength. However, a simple physical basis for the dependence of M_ρ on ρ is not understood.

The present development has the limitation that fibre breaks are assumed to be confined in a plane transverse to the fibre direction. Curtin (2000) has suggested that this assumption may lead to over-conservative predictions of composite strength. It is left to future work to extend the present approach to accommodate out-of-plane fibre breakage.

References

Alava MJ, Nukala PK, Zapperi S (2006) Statistical models of fracture. Advances in Physics 55(3-4):349–476

ASTM (2017) Standard test methods for tensile properties of polymer matrix composite materials. Standard D 3039, ASTM international, West Conshohocken PA

Batrouni GG, Hansen A, Nelkin M (1986) Fourier acceleration of relaxation processes in disordered systems. Physical review letters 57(11):1336

Beyerlein IJ, Phoenix SL, Sastry AM (1996) Comparison of shear-lag theory and continuum fracture mechanics for modeling fiber and matrix stresses in an elastic cracked composite lamina. International Journal of Solids and Structures 33(18):2543–2574

Cormen T, Leiserson C, Rivest R, Stein C (2001) Introduction To Algorithms. MIT Press

Curtin W (1998) Size scaling of strength in heterogeneous materials. Physical Review Letters 80(7):1445

Curtin W (2000) Dimensionality and size effects on the strength of fiber-reinforced composites. Composites Science and Technology 60(4):543–551

Daniels H (1945) The statistical theory of the strength of bundles of threads. i. Proc R Soc Lond A 183(995):405–435

Eaton JW, Bateman D, Hauberg S, Wehbring R (2015) GNU Octave version 4.0.0 manual: a high-level interactive language for numerical computations. CreateSpace Independent Publishing Platform, URL http://www.gnu.org/software/octave/doc/interpreter

Fidelis MEA, Pereira TVC, Gomes OdFM, de Andrade Silva F, Toledo Filho RD (2013) The effect of fiber morphology on the tensile strength of natural fibers. Journal of Materials Research and Technology 2(2):149–157

Gücer D, Gurland J (1962) Comparison of the statistics of two fracture modes. J Mech Phys Solids 10(4):365–373

Gupta A, Mahesh S, Keralavarma SM (2017a) A fast algorithm for the elastic fields due to a single fiber break in a periodic fiber-reinforced composite. International Journal of Fracture 204(1):121–127

Gupta A, Mahesh S, Keralavarma SM (2017b) Strength distribution of large unidirectional composite patches with realistic load sharing. Physical Review E 96:043,002

Gupta A, Mahesh S, Keralavarma SM (2018) A fast algorithm for the elastic fields due to interacting fibre breaks in a periodic fibre composite. International Journal of Fracture 211(1-2):295–303

Habeeb CI, Mahesh S (2015) Strength distribution of planar local load-sharing bundles. Physical Review E 92(2):022,125

Hedgepeth JM (1961) Stress concentrations in filamentary structures. Tech. Rep. TN D 882, NASA

Hedgepeth JM, Van Dyke P (1967) Local stress concentrations in imperfect filamentary composite materials. Journal of composite materials 1(3):294–309

Hull D, Clyne T (1996) An introduction to composite materials. Cambridge university press

Jawaid M, Khalil HA (2011) Cellulosic/synthetic fibre reinforced polymer hybrid composites: A review. Carbohydrate Polymers 86(1):1–18

Landis C, McMeeking R (1999) Stress concentrations in composites with interface sliding, matrix stiffness and uneven fiber spacing using shear lag theory. Int J Solids Struct 36(28):4333–4361

Landis CM, Beyerlein IJ, McMeeking RM (2000) Micromechanical simulation of the failure of fiber reinforced composites. Journal of the Mechanics and Physics of Solids 48(3):621–648

Mahesh S, Mishra A (2018) Strength distribution of ti/sic metal-matrix composites under monotonic loading. Engineering Fracture Mechanics 194:86–104

Mahesh S, Phoenix S (2004) Absence of a tough-brittle transition in the statistical fracture of unidirectional composite tapes under local load sharing. Phys Rev E 69(2):026,102

Mahesh S, Beyerlein IJ, Phoenix SL (1999) Size and heterogeneity effects on the strength of fibrous composites. Physica D: Nonlinear Phenomena 133(1):371–389

Mahesh S, Phoenix SL, Beyerlein IJ (2002) Strength distributions and size effects for 2d and 3d composites with weibull fibers in an elastic matrix. International Journal of Fracture 115(1):41–85

McCartney L, Smith R (1983) Statistical theory of the strength of fiber bundles. Journal of applied mechanics 50(3):601–608

Mishra A, Mahesh S (2017) A deformation-theory based model of a damaged metal matrix composite. Int J Solids Struct 121:228–239

Okabe T, Takeda N (2002) Elastoplastic shear-lag analysis of single-fiber composites and strength prediction of unidirectional multi-fiber composites. Compos A 33(10):1327–1335

Okabe T, Takeda N, Kamoshida Y, Shimizu M, Curtin W (2001) A 3D shear-lag model considering micro-damage and statistical strength prediction of unidirectional fiber-reinforced composites. Compos Sci Tech 61(12):1773–1787

Smith R (1980) A probability model for fibrous composites with local load sharing. Proc R Soc Lond A 372(1751):539–553

Smith R, Phoenix S, Greenfield M, Henstenburg R, Pitt R (1983) Lower-tail approximations for the probability of failure of three-dimensional fibrous composites with hexagonal geometry. Proc R Soc Lond A 388(1795):353–391

Tange O (2011) Gnu parallel - the command-line power tool. ;login: The USENIX Magazine 36(1):42–47, DOI http://dx.doi.org/10.5281/zenodo.16303, URL http://www.gnu.org/s/parallel

Weibull W (1951) A statistical distribution function of wide applicability. Journal of applied mechanics 103(730):293–297

Zhang J, Wang F (2009) Modeling of progressive failure in ductile matrix composites including local matrix yielding. Mech Adv Mater Struct 16(7):522–535

Zhou S, Curtin W (1995) Failure of fiber composites: a lattice green function model. Acta Metallurgica et Materialia 43(8):3093–3104